Initial evaluation of the use of USPIO cell labeling and noninvasive MR monitoring of human tissue-engineered vascular grafts *in vivo*

G. N. Nelson,* J. D. Roh,* T. L. Mirensky,* Y. Wang,* T. Yi,* G. Tellides,* J. S. Pober,* P. Shkarin,† E. M. Shapiro,† W. M. Saltzman,*,‡ X. Papademetris,†,‡ T. M. Fahmy,*,‡ and C. K. Breuer,*,[1]

*Interdepartmental Program in Vascular Biology and Therapeutics, School of Medicine; †Department of Radiology, School of Medicine; and ‡Department of Biomedical Engineering, Yale University, New Haven, Connecticut, USA

ABSTRACT **This pilot study examines noninvasive MR monitoring of tissue-engineered vascular grafts (TEVGs) *in vivo* using cells labeled with iron oxide nanoparticles. Human aortic smooth muscle cells (hASMCs) were labeled with ultrasmall superparamagnetic iron oxide (USPIO) nanoparticles. The labeled hASMCs, along with human aortic endothelial cells, were incorporated into eight TEVGs and were then surgically implanted as aortic interposition grafts in a C.B-17 SCID/bg mouse host. USPIO-labeled hASMCs persisted in the grafts throughout a 3 wk observation period and allowed noninvasive MR imaging of the human TEVGs for real-time, serial monitoring of hASMC retention. This study demonstrates the feasibility of applying noninvasive imaging techniques for evaluation of *in vivo* TEVG performance.—Nelson, G. N., Roh, J. D., Mirensky, T. L., Wang, Y., Yi, T., Tellides, G., Pober, J. S., Shkarin, P., Shapiro, E. M., Saltzman, W. M., Papademetris, X., Fahmy, T. M., Breuer, C. K.. Initial evaluation of the use of USPIO cell labeling and noninvasive MR monitoring of human tissue-engineered vascular grafts *in vivo*. *FASEB J.* 22, 3888–3895 (2008)**

Key Words: SCID/bg · animal model · arterial grafts · MRI

Tissue-engineered vascular grafts (TEVGs) hold great promise for advancing the fields of vascular and cardiovascular surgery. The translation of an autologous tissue-engineered conduit for use in congenital heart surgery marked an important milestone in the field of vascular tissue engineering (1–3). Further development of viable, autologous vascular grafts with the ability to repair and remodel could potentially benefit the estimated 80,000 patients per year in the United States who are not considered candidates for vascular bypass surgery due to lack of suitable autologous vessels and due to the poor function of currently available small-diameter synthetic vascular grafts (www.americanheart.org).

The most widely used approach for engineering tissues is to seed a synthetic polymer scaffold with living cells and, after some period of *ex vivo* culture, to then implant the construct into a living recipient. The original implant is often remodeled *in vivo*, resulting in a neotissue formed by the implanted cells, invading recipient cells, the residual scaffold, and an extracellular matrix (ECM) produced by the various cell populations within the graft. Despite the recent clinical translation of these technologies, little is known about the mechanisms underlying the formation of this vascular neotissue in TEVGs *in vivo* (4). Development of noninvasive imaging methods to assess implanted constructs could provide insight into this process and aid in the design of improved second-generation TEVGs. In addition, a noninvasive means of cell-surveillance could provide physicians with a valuable tool for monitoring the development and function of these grafts in the clinical setting. To this end we have developed an approach using ultrasmall superparamagnetic iron oxide (USPIO) nanoparticles to label human aortic smooth muscle cells (hASMCs). The labeled cells were seeded onto a biodegradable tubular scaffold fabricated from poly-L-lactic acid (PLA) nonwoven felts coated with a 50:50 copolymer of ε-caprolactone and L-lactide [P(CL/LA)]. After 6 days in culture, the lumen of the labeled scaffold was seeded with human aortic endothelial cells (hAECs). After an additional 24 h in culture, the seeded, labeled tissue-engineered constructs were surgically implanted as aortic interposition grafts in female severe combined immunodeficient/beige (SCID/bg) mouse recipients. Magnetic resonance imaging was used to evaluate the structure and function of the human TEVGs in addition to investigating the fate of the cells *in vivo* over a 3-wk time course.

[1] Correspondence: Yale University School of Medicine, Interdepartmental Program in Vascular Biology and Therapeutics, Amistad Research Bldg., 10 Amistad St., Rm. 301B, P.O. Box 208089, New Haven, CT 06520, USA. E-mail: christopher.breuer@yale.edu

doi: 10.1096/fj.08-107367

0892-6638/08/0022-3888 © FASEB

To produce an identifiable change in signal intensity, the cells of interest were labeled with USPIO nanoparticles, an established MR contrast agent with proven clinical safety and efficacy (5, 6). These T2 contrast agents shorten T2 relaxation times, which results in a hypodense signal and negative image. USPIO contrast agents produce a greater signal change than paramagnetic contrast agents, such as gadolinium, which thereby allows a more robust and efficient detection of small numbers of cells (7). MR imaging of USPIO labeled cells has been used successfully to track cells transplanted in preclinical and clinical studies investigating cellular therapy for the treatment of demyelinating diseases, spinal injuries, cerebral ischemia, and myocardial infarction (7–12). Cell labeling prior to implantation allows for monitoring cellular biodistribution *in vivo*. The major advantage of imaging USPIO labeled cells is that it provides high-spatial resolution and the potential to repeatedly image the same subject over time, enabling visualization and evaluation of cellular survival and integration *in vivo*. In addition, since the USPIO particles contain iron, they can also be visualized in conventional tissue sections using Prussian blue staining. Thus, MR data can be correlated and validated histologically.

MATERIALS AND METHODS

Graft production

PLA nonwoven felts were used for the framework of the scaffold (Concordia Fibers, Coventry, RI, USA) and coated in P(CL/LA as previously reported (13). PLA felts were 300 μm thick with ~83% total porosity. Felts were shaped into tubes by introducing 10.0 × 4.0 mm sections into the inlet of a cylinder with an internal diameter of 1.4 mm. Stainless steel 22-gauge needles were then introduced into the opposing end to maintain the inner lumen and compress the felt. A 5% (w/v) P(CL/LA) (263.8 kDa; Absorbable Polymers International, Birmingham, AL, USA) in glacial acetic acid sealant solution was injected into the inlet of the chamber system and allowed to penetrate the felt. These hybrid polyester scaffolds were frozen at –20°C for 30 min and lyophilized for 24 h, which resulted in PLA-P(CL/LA) scaffolds with an internal diameter of 0.9 mm and wall thickness of 250 μm, as previously reported (5). Total porosity of the PLA-P(CL/LA) scaffolds was 60.4%. The mean pore size was 31.2 ± 16.1 μm for the PLA-P(CL/LA) scaffold. Initial tensile strength and elastic modulus of the scaffold were 3.7 ± 0.53 and 24 ± 5.9 MPa. The resultant burst pressure of the PLA-P(CL/LA) scaffolds was 2790 ± 180 mmHg, and its suture retention strength was 4.37 ± 0.67 N, as previously reported (13).

Cell culture

hASMCs (Lonza, Inc., Allendale, NJ, USA) were cultured in an SMC-specific medium (SmGM-2, Smooth Muscle Growth Medium 2, Lonza) and harvested between passages 4 and 8 for all seeding experiments. hAECs (Lonza) were cultured in an EC-specific medium (EGM-2, Endothelial Growth Medium 2, Lonza) and harvested between passages 6 and 8.

Cell seeding and *in vitro culture*

Each PLA-P(CL/LA) scaffold was trimmed to 4 mm in length and sterilized *via* incubation at 20°C under UV light in an antibiotic solution of 10% (v/v) penicillin/streptomycin in sterile PBS. Scaffolds were washed in sterile PBS prior to seeding. hASMCs were trypsinized and collected for seeding in SmGM-2. Approximately 1×10^6 cells in 10 μl of medium were seeded onto each scaffold by clamping one end of the scaffold and pipetting the cell suspension into the lumen through the opposite end. The scaffold was then gently compressed to encourage cell infiltration into the porous walls. This process of pipetting and compression was repeated 3 times at each end of the scaffold. Each seeded scaffold was then allowed to sit for ~10 min to allow cell adhesion. A 25-gauge needle was then gently threaded through the lumen of the graft, to prevent occlusion *via* cellular ingrowth, and each graft was incubated for 6 days in 3 ml of SmGM-2, with medium changes every 2 to 3 days. On day 6, the 25-gauge needle was removed, and one end of the graft was clamped with microsurgical vascular clips. Approximately $2.0–2.5 \times 10^5$ hAECs in 2.0–2.5 μl of EGM-2 were then pipetted into the lumen of the graft. Each graft was allowed to sit for 10 min for EC adhesion before submersion in EGM-2 for 24 h prior to surgical implantation on day 7.

USPIO nanoparticle preparation

Commercially available USPIO nanoparticles (Combidex, AMAG Pharmaceuticals, Inc., Cambridge, MA, USA) were incubated with a solution of high-molecular-weight poly-L-lysine (Sigma-Aldrich, St. Louis, MO, USA) on an orbital shaker for 1 h as follows: 30 mg of Combidex nanoparticles was added to 15 ml of serum-free high-glucose Dulbecco's modified Eagle medium (DMEM; Invitrogen, Carlsbad, CA, USA). This solution was mixed with 1.8 mg of poly-L-lysine dissolved in 15 ml of high-glucose DMEM, which produced 30 ml of stock solution containing USPIO and poly-L-lysine concentrations of 1000 μg/ml and 60 μg/ml, respectively. This ratio of USPIO to poly-L-lysine was held constant throughout all serial dilution studies.

Prussian blue staining and labeling efficiency determination

Approximately 140,000 hASMCs were plated into each well of a 6-well tissue culture plate. SmGM-2 (3 μl) was added to each well, and the cells were incubated overnight (12–16 h) with poly-L-lysine-coated USPIO nanoparticles at each of the following iron concentrations: 0, 25, 50, 100, and 250 μg/ml. The following day, the cells were washed 3 times with PBS, trypsinized, and plated onto sterile microscope coverslips. Once adherent, the cells were fixed in 10% neutral buffered formalin (NBF; Sigma-Aldrich) overnight and stained for the presence of intracellular iron. Potassium ferrocyanate (4% w/v in distilled water) was mixed with a 20% w/v solution of hydrochloric acid. Samples were exposed to a fresh preparation of this mixture for 20–30 min before being washed 3 times with distilled water. Cells were then counterstained with nuclear fast red counterstain (Sigma-Aldrich) at room temperature for 5–10 min. Labeling efficiencies were determined by counting the first 100 to 200 cells and then calculating the fraction of these cells staining positive for Prussian blue.

Cell metabolism assays

In order to determine hASMC metabolic activity following USPIO-labeling, CellQuanti-MTT assays (BioAssay Systems, Hayward, CA, USA) were performed. Briefly, ~11,000 cells in

80 μl of SmGM-2 were plated to the wells of a 96-well plate. Once adherent, these cells were incubated with USPIO overnight, washed, and cultured in 80 μl of SmGM-2. MTT (15 μl) reagent [3-(4,5-dimethyl-2-thiazolyl)-2,5-diphenyltetrazolium bromide] was then added to each well and allowed to incubate for 4 h at 37°C. Following incubation, 100 μl of solubilization buffer was then added, and absorbances were determined *via* spectrometry at 570 nm. The relative cell metabolism was determined as the ratio of absorbance from wells incubated with USPIO to the control well (receiving a USPIO concentration of 0 μg/ml). Experiments were performed in triplicate.

Label retention study

In order to determine label retention with time, labeled cells were grown *in vitro* through 5 wk. Cells at each week were plated to sterile coverslips, fixed in NBF, and stained *via* Prussian blue as described above. The label retention fraction was calculated as: (number of cells among the first 100–200 cells counted that stained positive for Prussian blue)/(number of cells counted).

***In vitro* T2 quantification *vs.* time**

In order to determine how relaxation time changes with cell replication, 10^5 cells were plated into four separate T25 flasks and exposed to 250 μg Fe/ml overnight. Medium was changed every 2 days. Labeled cells were then collected and counted at each of 4, 7, 11, 14, 18, and 21 days. Following collection and counting, labeled cells were suspended in 400–500 ml of Histogel® (Richard-Allan Scientific, Kalamazoo, MI, USA) within 0.5 ml Eppendorf tubes. MRI was performed using a Bruker 4T small-animal imager with an inner diameter of 16 cm. Multispin multiecho images were obtained with the following MR parameters: FOV = 2.56 cm^2, matrix = 64 × 64, number of echoes = 8, and echo spacing = 15 ms. Each time point was performed in triplicate or quadruplicate.

MR imaging of gelatin graft suspensions

On day 1 postseeding, one graft seeded with USPIO-labeled hASMCs was suspended in Histogel within a Microtainer tube (BD Biosciences, San Jose, CA, USA). As controls, one Microtainer tube filled with only Histogel and one containing an unlabeled, seeded scaffold were imaged concurrently. We acquired multispin multiecho images (FOV=4.0 mm×4.0 mm, matrix=128×128, number of echoes=6, echo spacing=3.59 ms), in both coronal and axial planes.

Surgical implantation

Female C.B-17 SCID/bg mice ages 8 to 12 wk underwent surgical implantation of the human TEVGs as previously reported (5). Animal handling was in accordance with the institutional guidelines for the use and care of animals, and the institutional review board approved the experimental procedures. Briefly, mice were anesthetized with intraperitoneal injection made by mixing 1.5 ml of 100 mg/ml xylazine (Sigma-Aldrich) and 10 ml of 100 mg/ml ketamine (Sigma-Aldrich) diluted in a ratio of 1:4 with 0.9% normal saline and injected at a dose of 0.1 ml/20 g of body weight. Using an ×18 dissecting microscope (Zeiss, Thornwood, NY, USA), a midline laparotomy was performed, and the abdominal viscera were lateralized to allow visualization of the abdominal aorta. Care was taken to separate the aorta from the vena cava. Proximal and distal vascular control of the vessels was obtained below the renal vessels and above the iliac bifurcation. The open abdominal cavity was bathed in warmed (37°C) heparinized saline (250 U/ml). The native vessel was gently occluded with removable microvascular clamps and then transected. Anastamosis to a caliber-matched TEVG (~1 mm diameter) was performed using interrupted 10-0 monofilament nylon (Sharpoint Lab Sutures, Calgary, AB, Canada). On completion of the distal anastamosis, the midline incision was closed with running 5-0 prolene sutures. After laparotomy closure, animals were monitored during recovery and placed on a warm pad to avoid hypothermia. The animals recovered quickly. None of the mice displayed hind limb dysfunction postoperatively. A total of 8 TEVGs (~1 mm in diameter and 3 mm in length) were implanted as aortic interposition grafts. The grafts were excised between 4 and 18 days postoperatively.

***In vivo* MR imaging**

On days 4, 11, and 18, SCID/bg mice with seeded and unseeded scaffolds underwent MR imaging. These mice were either anesthetized and resuscitated or euthanized prior to imaging. The anesthesia protocol consisted of pretreatment with an intraperitoneal injection made by mixing 1.5 ml of 100 mg/ml xylazine and 10 ml of 100 mg/ml ketamine diluted in a ratio of 1:4 with 0.9% normal saline and injected at a dose of 0.1 ml/20 g of body weight. Anesthetized mice were intubated and maintained on isofluorane for gated MR imaging. Euthanized mice were sacrificed *via* CO_2 asphyxiation prior to imaging. Mice underwent imaging as described above. One mouse with an unseeded PLA scaffold was used as a control for this study.

T2 value calculations

We computed quantitative relaxation-time (T2) maps of the tissue by fitting a monoexponential model to the multispin multiecho images using the Yale Bioimage Suite software package (www.bioimagesuite.org). From the T2 maps, the values of 20 sample pixels along the walls of each graft were averaged to produce representative T2 ± SD values for all imaged specimens.

Histology and immunohistochemistry

Seeded and unseeded scaffolds were all explanted and fixed in NBF prior to histological embedding with either glycol-methacrylate (GMA) or paraffin. GMA-embedded samples were stained with Lee's methylene blue as a substitute for traditional hematoxylin and eosin (H&E) staining. Paraffin samples were prepared for Voerhoeff-van Gieson elastin staining (Sigma-Aldrich) and immunohistochemical identification of vascular and inflammatory cells, using the following antibodies: anti-human α-smooth muscle actin (α-SMA; Dako North America, Inc., Carpinteria, CA, USA), anti-human CD31 (Dako), anti-rabbit von Willebrand's Factor (vWF; Dako), anti-mouse isolectin IB4 (Vector Laboratories, Burlingame, CA, USA), and anti-mouse Mac3 (BD Biosciences) antibodies.

Statistical analysis

T2 values from *in vivo* USPIO-labeled and unlabeled grafts were analyzed with paired and unpaired Student's *t* tests. Values of $P < 0.05$ were considered statistically significant.

RESULTS

Analysis of tissue-engineered vascular grafts *in vitro*

We created polyester tubular scaffolds with sufficient wall strength and of a diameter suitable for interposition into the infrarenal aorta of an immunodeficient mouse. We then tested whether unlabeled hASMCs could be used to seed our synthetic polymer scaffold *in vitro*. As shown in **Fig. 1*A, B***, grafts seeded and cultured with hASMCs display a high degree of cellularity on the luminal surface, within the wall, and on the exterior of the scaffold.

Cell labeling and *in vitro* MRI analysis

Before creating labeled grafts for *in vivo* MRI, we investigated the labeling of hASMCs. To label cells for *in vitro* MR imaging, hASMCs were incubated with poly-L-lysine-coated USPIO nanoparticles at five serially diluted concentrations from 0 to 250 μg/ml. After Prussian blue staining to reveal intracellular iron deposits, labeling efficiencies were greater than 95% for every concentration of USPIO nanoparticles, reaching 100% at higher concentrations (**Table 1**, Fig. 1*C–F*). One day after particle addition, the early cell metabolic activities at serial concentrations of USPIO nanoparticles, as revealed by an MTT assay, were not statistically different from those of control specimens (Table 1). Labeled cells grown for 5 wk postimplantation were stained *via* Prussian blue at the conclusion of each week, revealing label retentions greater than 95% at late time points, although the strength of the Prussian blue stain decreased each week (**Table 2**).

Labeled cells were then expanded in culture for 3 wk

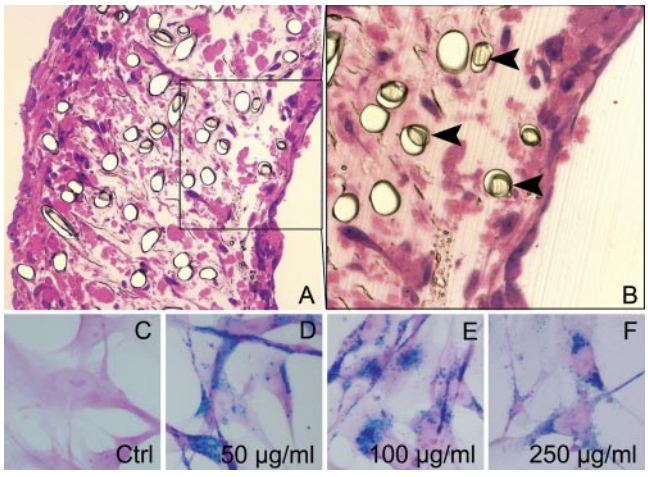

Figure 1. Evaluation of cell seeding *in vitro*. *A*) Photomicrograph of hASMCs statically seeded on scaffold *in vitro*, day 6 (H&E; ×20). *B*) Photomicrograph of hASMCs statically seeded on scaffold *in vitro*, day 6 (H&E; ×40). Note cellular material interspersed among residual polymer fibers (black arrowheads). *C–F*) Photomicrographs of SMCs (Prussian blue; ×40): unlabeled control (*C*); labeled with 25 μg USPIO/ml (*D*), 50 μg USPIO/ml (*E*), 100 μg USPIO/ml (*F*).

TABLE 1. *Cell viability and labeling efficiency, 1 day postlabeling*

USPIO concentration (μg/ml)	Metabolic activity	Labeling efficiency (%)
0	1.000	1.5
25	0.907 ± 0.19	99.5
50	0.809 ± 0.241	100
100	0.824 ± 0.076	100
250	0.749 ± 0.15	99.5
500	0.898 ± 0.022	100

Activity values are means ± SD; $n = 4$.

in order to investigate the effects of cell replication on signal intensity. We found that labeled hASMCs grown *in vitro* underwent ~6.6 population doublings in 21 days, with moderate increases in *in vitro* T2 values. However, the mean T2 value for all unlabeled samples (**Table 3**, **Fig. 2*A***) was 96.25 ± 12.26, a significantly higher value (almost double) than the mean for all labeled samples. Labeled T2 mean values ranged between 41.75 ± 0.5 and 61.33 ± 4.93 (mean 51.17±8.08) throughout the time course (Fig. 2). The consistently low T2 values of labeled cells *in vitro* suggest that poly-L-lysine-coated USPIO nanoparticles have been retained within cells and are relatively stable, although the increase in signal suggests that they have undergone some degree of intracellular Fe metabolism.

Next, we proceeded to use USPIO-labeled hASMCs to seed scaffolds for *in vitro* MR analysis. Two scaffolds, one seeded with cells labeled with USPIO at 250 μg/ml and one seeded with unlabeled cells, were embedded in Histogel for MR analysis. Labeling with USPIO significantly reduced the signal intensity of the scaffold and, due to its "blooming" effect, of the immediately surrounding gelatin (**Fig. 3*A, B***). The unlabeled, seeded PLA tissue-engineering scaffold produced several small areas of low-signal intensity. However, following USPIO-labeled cell seeding, the scaffold was uniformly dark and easily identifiable. Overall, *in vitro* T2 values were significantly higher in unlabeled grafts (**Table 4**).

Graft characterization *in vivo*

Mice received either seeded and labeled or unseeded TEVGs and were then serially imaged by MR. Postoperatively, each of the 8 SCID/bg mice exhibited good

TABLE 2. *USPIO label retention at 250 μg/ml*

	Label retention	
Passage	Fraction	Percentage
0	200/200	100
3	197/200	98.5
4	187/200	93.5

$n = 3$.

TABLE 3. *T2 values with in vitro* cell replication

Duration (days)	Population doublings	Unlabeled T2	Labeled T2
4	2.62	–	50.75 ± 1.5[a]
7	4.14	89	41.75 ± 0.5[b]
11	4.79	83	42 ± 4.24[b]
14	5.61	104	56.5 ± 4.36[b]
18	5.52	109	57.25 ± 1.5[b]
21	6.63	–	61.33 ± 4.93[a]
Mean		96.25 ± 12.26[b]	

Labeled T2 and mean unlabeled T2 values are means ± SD. [a]n = 3. [b]n = 4.

hind limb function, an early indicator of aortic graft patency. *In vivo*, the grafts were easily identified in a retroperitoneal and infrarenal location at 4, 11, and 18 days postimplantation (representative images shown in Fig. 3*C–E*). T2 values, calculated from the latter scanning sequence, revealed that USPIO-labeled TEVGs consistently appeared with sharper borders and registered lower T2 values than the unseeded, unlabeled control scaffold *in vivo*. These data are represented qualitatively and visually as T2 maps in Fig. 3*D, F* and quantitatively in Table 4.

To aid in the interpretation of the MR images, grafts were harvested at 3 wk postimplantation and analyzed by both conventional histology and immunohistochemistry. On gross examination, none of the 8 grafts (seeded or unseeded) displayed evidence of occlusion, rupture, or aneurysm formation, achieving 100% patency for at least 3 wk *in vivo*. Conventional histology revealed increased subendothelial matrix deposition at 11 days with a few scattered nuclei (not shown); histology at 18 days displayed increased cellularity and organization (**Fig. 4*A***). Staining for extracellular collagen revealed robust ECM deposition in early stages of graft development, correlating to the increased cellularity. Voerhoeff-van Gieson stains were unreactive, suggesting little to no elastin deposition within our TEVGs at these early time points (data not shown).

Immunohistochemical detection of α-SMA revealed that much of the intramural cell population was α-SMA positive, indicating that these cells were either SMCs or myofibroblasts (Fig. 4*B*). Concomitant Prussian blue staining revealed colocalization of both the α-SMA and Prussian blue signals (red arrowheads), suggesting that our USPIO-labeled hASMCs persisted within the graft wall at 18 days postimplantation. Identification of murine inflammatory cells *via* anti-Mac3 and Prussian blue staining (Fig. 4*C*) revealed that a modest proportion of the USPIO nanoparticles was within macrophages (purple arrowheads). However, most of the iron oxide label was retained within seeded hASMCs.

Immunohistochemical staining with anti-rabbit vWF, which reacts with both human and mouse ECs, was positive in all samples, which verified the presence of an endothelial lining for up to 18 days (Fig. 4*D*). Anti-human CD31 staining (specific for human ECs) was weakly positive in 4-day samples (not shown), verifying the presence of a portion of the seeded human ECs. However, in all samples after 4 days, anti-hCD31 staining was absent (Fig. 4*E*). On the contrary, the 18-day samples were positive for IB4 (a mouse-specific endothelial marker) (Fig. 4*F*), suggesting that seeded hAECs were replaced by murine ECs within the first week after implantation.

DISCUSSION

This study uses cellular MR imaging techniques aimed at noninvasively visualizing the viability of TEVGs in a living animal (7). To accomplish this, we optimized cell uptake by using poly-L-lysine-coated USPIO particles (7). Poly-L-lysine, which facilitates entry into cells, has been shown to improve uptake in many cell types (6, 14–16). Adverse effects on cell function are possible, although we observed none in our work. No significant toxic effects have been reported in the referenced literature; however, it has been shown that differentiation of mesenchymal cells into chondrocytes is inhibited by USPIO labeling (17). As in previous investigations, we used an MTT assay, which measures cell

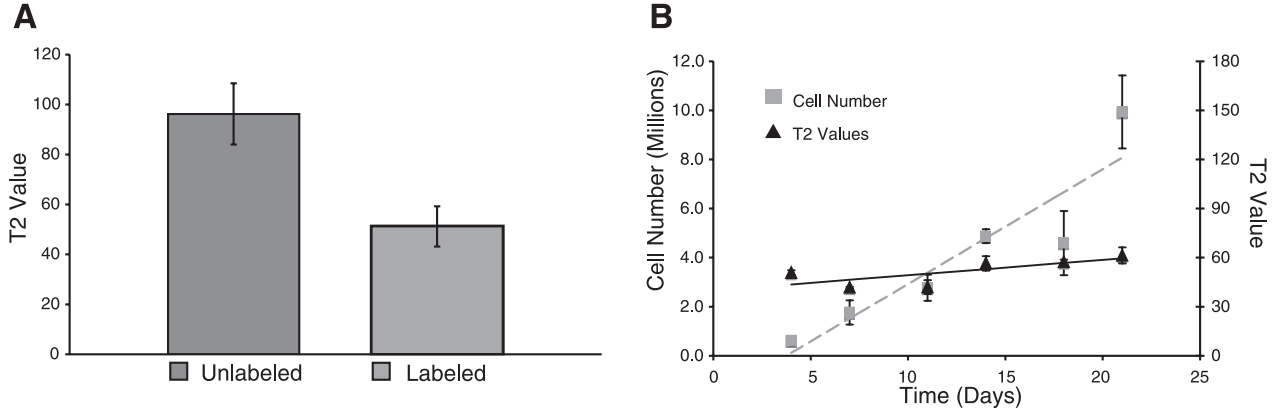

Figure 2. T2 Values with *in vitro* cell replication. *A*) Mean unlabeled *vs.* mean labeled cell T2 values. *B*) Labeled cell T2 values and cell population number plotted against time.

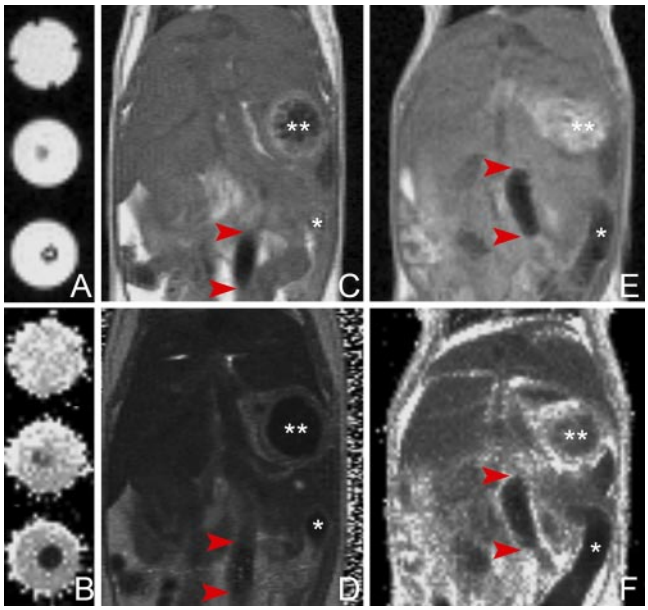

Figure 3. Imaging of USPIO-labeled grafts *in vitro* and *in vivo*. *A*) T2 Spin Echo sequence imaging of a gelatin phantom (top), an unlabeled PLA-P(CL/LA) scaffold (middle), and an USPIO-labeled scaffold (bottom). *B*) T2 mapping of the same three specimens. *C*) Representative image of *in vivo* scaffold MR imaging from an unseeded 18-day specimen in the aortic position. Note blurred edges of graft delineated by red arrows. Single asterisk indicates air in large bowel. Double asterisks indicate air in stomach. *D*) T2 mapping of the same specimen. *E*) T2 spin echo image of an 18-day USPIO-labeled scaffold. Note sharp edges of graft delineated by red arrows. Single asterisk indicates air in large bowel. Double asterisks indicate fluid in stomach. *F*) T2 mapping of the same specimen.

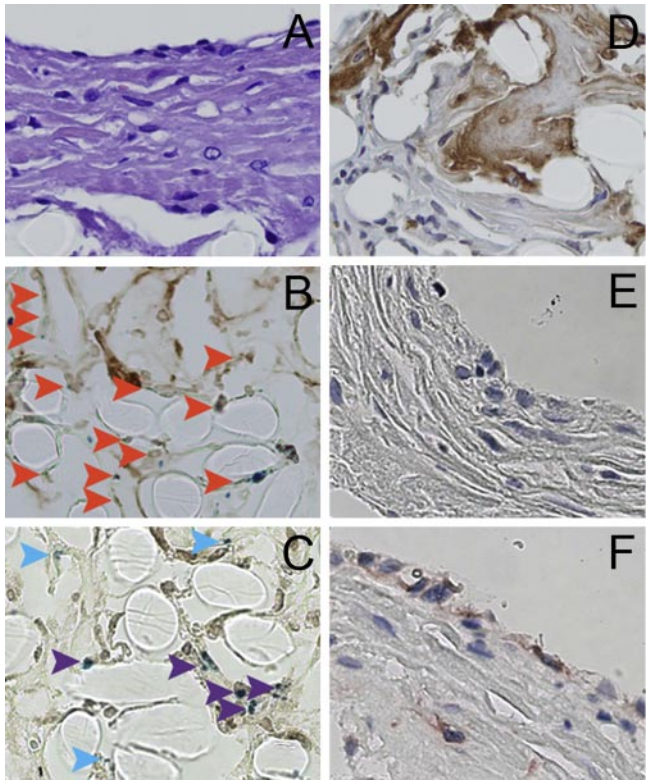

Figure 4. Photomicrographs of histology and immunohistochemistry performed on 18-day labeled, seeded scaffolds (×400). *A*) H&E. *B*) Anti-α-SMA with Prussian blue; red arrows mark colocalizing signals. *C*) Anti-mouse Mac3 with Prussian blue; purple arrows mark colocalizing signals, blue arrows mark Prussian blue not associated with macrophages. *D)* Anti-vWF. *E*) Anti-human CD31. *F*) Anti-mouse isolectin IB4.

metabolic activity, as a test for cell viability. In this study we found that cell metabolism was not substantially reduced immediately following labeling, even at very high concentrations (250 μg/ml).

Another potential pitfall of USPIO particles is their blooming effect (10, 18–22). The magnetic susceptibility of USPIO affects an area larger than the actual size of the particles, leading to exaggeration of the region occupied by iron oxide in the image generated. Well-designed labeling techniques and pulse sequences in the MRI process can improve resolution by minimizing this effect (19). An additional potential limitation of the use of USPIO labeling is that little is known about the long-term stability of the iron oxide compounds. It is presumed that any iron atoms released from particles are incorporated into the normal iron turnover inside the cell (7). Some investigators have suggested that metabolism of USPIO particles occurs *via* lysosomal degradation pathways and that iron released from endosomes is scavenged intracellularly by ferritin (23, 24). Nanoparticle phagocytosis by macrophages could, however, lead to detection of the metabolic breakdown and elimination of USPIO rather than labeled cells. If this is the case, the local relaxation times should increase due to degradation of the magnetic label. It has been reported that the half-life of phagocytosed USPIO is only 8 days (25). If this form of degradation was a prominent cellular mechanism in our study, our T2 signal should increase dramatically over 18 days (~2.25 half-lives). Because no statistically significant change was detected in *in vivo* T2 values of labeled TEVGs, we therefore conclude that little macrophage-mediated degradation occurred. More studies are needed to accurately determine the fate of the contrast agents *in vivo*; both to determine any potential adverse effects and to determine their reliability as cellular imaging agents of targets of interest.

To date, only limited work has been performed

TABLE 4. *T2 values*

Treatment	*In vivo* duration	T2 value
In vitro grafts		
Seeded/labeled		26.93 ± 6.37
Seeded/unlabeled		87.04 ± 11.53
In vivo grafts		
Seeded/labeled	11 days	26.32 ± 2.24
	18 days	
	Specimen 1	25.22 ± 2.96
	Specimen 2	25.70 ± 3.69
Unseeded/unlabeled	18 days	35.30 ± 2.66

Values are means ± SD.

applying MR cellular imaging techniques to investigate cellular behavior in tissue engineering applications. Terrovitis *et al.* (26) investigated the use of MRI-visualized SPIO-labeled human mesenchymal stem cells (hMSCs) in tissue-engineered heart valves *in vitro*. Seeded collagen gels were serially imaged *in vitro* using MRI over a 4 wk time course. The authors concluded that SPIO labeling did not cause any adverse effects on the functional properties of the cells and that the labeled cells can effectively be visualized within collagen gels *in vitro* using MRI. Ko *et al.* (27) then demonstrated the feasibility of using SPIO-labeled cells for cell surveillance in tissue-engineered constructs *in vivo*. In this study, the investigators seeded and cultured SPIO-labeled bone marrow-derived hMSCs on gelatin sponges *in vitro*, implanted the tissue-engineered constructs subcutaneously into nude mice, and serially imaged the tissue-engineered constructs *in vivo* using MRI over a 4 wk time course. The investigators demonstrated their ability to detect the labeled cells both *in vitro* and *in vivo* using MR, confirmed these findings histologically using Prussian blue, and concluded that MRI could be used to noninvasively determine the fate of transplanted cells and observe their behavior around the scaffold *in vivo*.

In this investigation, we demonstrated that USPIO labeling could be used to enhance noninvasive imaging of vascular tissue engineering constructs. The USPIO label was readily taken up by the hASMCs and did not affect short-term cell viability, as determined by an MTT assay. The cells retained their label through 5 wk *in vitro*, as confirmed histologically *via* Prussian blue staining. *In vitro* culture of labeled cells revealed that the USPIO label maintains its effect, evidenced by consistently low T2 values, despite a 99-fold increase in cell number (Table 3, Fig. 2). Using a human TEVG created by seeding labeled hASMCs onto a tubular PLA-P(CL/LA) scaffold, we demonstrated retention of the USPIO label for 3 wk *via in vivo* T2 quantification, Prussian blue staining, and immunohistochemistry.

Combining these data with the stable *in vivo* T2 values (Table 4), we conclude that a majority of the USPIO label has been retained within the TEVG, facilitating a noninvasive monitoring method of the graft. Though we have some histological evidence of macrophage phagocytosis and cannot rule out USPIO metabolism or hASMC migration out of grafts (all possible complicating factors), these three scenarios should produce significant increases in the TEVG T2 signal. Therefore, our *in vivo* TEVG T2 values, unchanged over nearly 3 wk, suggest that these processes exerted little influence over our imaging results. Furthermore, histological assessment supports this conclusion: Seeded hASMCs attached to the tubular scaffold and became incorporated into the neomedia of the TEVG, as confirmed by demonstrating that neomedial cells colocalized for both α-SMA and Prussian blue. While more work is needed to fully evaluate these findings, our initial study does suggest that USPIO labeling and MR imaging has great potential for verifying the retention of implanted cells in functional tissue-engineered vascular grafts.

Compared to other imaging technologies used in determining cell fate, USPIO nanoparticles possess distinct advantages. Most significantly, MR is already widely used clinically for structural and physiological evaluation of anatomic structures. In fact, MR analysis of cardiovascular structures provides excellent soft tissue contrast, enabling high anatomic detail. The use of USPIO labeling in MRI will enhance these capabilities by providing additional data that can be used to elucidate the mechanisms underlying vascular neotissue formation *in vivo*. In contrast, longitudinal bioluminescence imaging (BLI), a competing cell-surveillance technology, requires both genetic alteration of the cell of interest and the administration of an enzymatic substrate in order to produce a signal that can be traced (28, 29). Concerns surrounding the effect of genetic transfection on the function of experimental cells and the efficacy of future cell-based therapies must be addressed in detail in order for these technologies to achieve a significant role in monitoring implanted cells in a clinical setting. In addition, BLI techniques are severely limited in their depth of penetration (29). Firefly luciferace, a commonly utilized enzyme, activates its substrate, luciferin, to emit light with a wavelength peak at 560 nm. Light in this range is scattered by solid tissues and absorbed by hemoglobin, lipids, and water, leading to serious attenuation of the luminescent signal at depths greater than 7 cm (29). In contrast to BLI, positron emission tomography (PET) and single-photon emission computed tomography (SPECT) are prominent imaging modalities commonly used in cell tracking that possess better signal penetrance, allowing the assessment of tissues at a wider range of anatomic locations. When compared to MRI, these two technologies, like BLI, provide useful information regarding physiological function but lack the ability to provide structural data (30). In addition, PET and SPECT carry the added drawbacks of exposure to ionizing radiation, considerations that currently limit the use of these technologies in certain patient populations, such as children. Furthermore, MRI temporal resolution, on the order of milliseconds, is more than 2-fold greater than PET and an order of magnitude better than SPECT (30).

For these reasons, the use of MR to noninvasively monitor implanted TEVGs and evaluate seeded cell retention provides a unique combination of characteristics that are useful in investigating vascular neotissues in therapeutic settings. The value of this technology is only enhanced by the fact that it can be accomplished in any clinically relevant anatomic location with simultaneous demonstration of structure and function. MR techniques, combined with USPIO, are already proving useful in our laboratory effort to understand the cellular behavior underlying vascular tissue engineering applications and design the next generation of human TEVGs. In the future, this noninvasive method for evaluating neotissue development and graft function *in*

vivo may also provide a powerful tool for monitoring TEVG development and function in clinical settings.FJ

We thank Nancy Troiano and Chris Coady for their help in GMA and paraffin embedding. This work was supported by grants from the U.S. National Institutes of Health (NIH; K08HL83980–2, R01 EB006494–01 P01-HL070295), the American Surgical Association, the Yale University Office of Student Research, and the Yale University Department of Surgery Ohse Grant Program. In addition, this work was performed as part of an NIH-sponsored Howard Hughes Medical Institute Medical Research Training Fellowship. The authors declare they have no competing financial interests.

REFERENCES

1. Shin'oka, T., Imai, Y., and Ikada, Y. (2001) Transplantation of a tissue-engineered pulmonary artery. *N. Engl. J. Med.* **344,** 532–533
2. Matsumura, G., Hibino, N., Ikada, Y., Kurosawa, H., and Shin'oka, T. (2003) Successful application of tissue engineered vascular autografts: clinical experience. *Biomaterials* **24,** 2303–2308
3. Shin'oka, T., Matsumura, G., Hibino, N., Naito, Y., Watanabe, M., Konuma, T., Sakamoto, T., Nagatsu, M., and Kurosawa, H. (2005) Midterm clinical results of tissue-engineered vascular autografts seeded with autologous bone marrow cells. *J. Thorac. Cardiovasc. Surg.* **129,** 1330–1338
4. Matsumura, G., Miyagawa-Tomita, S., Shinoka, T., Ikada, Y., and Kurosawa, H. (2003) First evidence that bone marrow cells contribute to the construction of tissue engineered vascular autografts in vivo. *Circulation* **108,** 1729–1734
5. Runge, V. M. (2000) Safety of approved MR contrast media for intravenous injection. *J. Magn. Reson. Imaging* **12,** 205–213
6. Breslau, J., Jarvik, J. G., Haynor, D. R., Longstreth, W. T. Jr., Kent, D. L., and Maravilla, K. R. (1999) MR contrast media in neuroimaging: a critical review of the literature. *Am. J. Neuroradiol.* **20,** 670–675
7. Modo, M., Hoehn, M., and Bulte, J. (2005) Cellular MR imagine. *Mol. Imaging* **4,** 143–164
8. Anderson, S. A., Shukaliak-Quandt, J., Jordan, E. K., Arbab, A. S., Martin, R., McFarland, H., and Frank, J. A. (2004) Magnetic resonance imaging of labeled T-cells in a mouse model of multiple sclerosis. *Ann. Neurol.* **55,** 654–659
9. Hoehn, M., Küstermann, E., Blunk, J., Wiedermann, D., Trapp, T., Wecker, S., Föcking, M., Arnold, H., Hescheler, J., Fleischmann, B. K., Schwindt, W., and Bührle, C. (2002) Monitoring of implanted stem cell migration in vivo: a highly resolved in vivo magnetic resonance imaging investigation of experimental stroke in rat. *Proc. Natl. Acad. Sci.* **99,** 16267–16272
10. Shapiro, E. M., Skrtic, S., and Koretsky, A. P. (2005) Sizing it up: cellular MRI using micron-sized iron oxide particles. *Magn. Reson. Med.* **53,** 329–338
11. Zhang, Z. G., Jiang, Q., Zhang, R., Zhang, L., Wang, L., Zhang, L., Arniego, P., Ho, K. L., and Chopp, M. (2003) Magnetic resonance imaging and neurosphere therapy of stroke in rat. *Ann. Neurol.* **53,** 259–263
12. Zhang, R. L., Zhang, L., Zhang, Z. G., Morris, D., Jiang, Q., Wang, L., Zhang, L. J., and Chopp, M. (2003) Migration and differentiation of adult rat subventricular zone progenitor cells transplanted into the adult rat striatum. *Neuroscience* **116**, 373–382
13. Roh, J. D., Nelson, G. N., Brennan, M. P., Mirensky, T. L., Yi, T., Hazlett, T., Tellides, G., Sinusas, A. J., Pober, J. S., Saltzman, W. M., Kyriakides, T. R., and Breuer, C. K. (2008) Small-diameter biodegradable scaffolds for functional vascular tissue engineering in the mouse model. *Biomaterials* **29,** 1454–1463
14. Kraitchman, D. L., Heldman, A. W., Atalar, E., Amado, L. C., Martin, B. J., Pittenger, M. F., Hare, J. M., and Bulte, J. W. (2003) In vivo magnetic resonance imaging of mesenchymal stem cells in myocardial infarction. *Circulation* **107,** 2290–2293
15. Anderson, S. A., Glod, J., Arbab, A. S., Noel, M., Ashari, P., Fine, H. A., and Frank, J. A. (2005) Magnetic resonance imaging of labeled T-cells in a mouse model of multiple sclerosis. *Blood* **105,** 420–425
16. Kostura, L., Kraitchman, D. L., Mackay, A. M., Pittenger, M. F., and Bulte, J. W. (2004) Feridex labeling of mesenchymal stem cells inhibits chondrogenesis but not adipogenesis or osteogenesis. *NMR Biomed.* **17,** 513–517
17. Bulte, J. W., Kraitchman, D. L., Mackay, A. M., and Pittenger, M. F. (2004) Chondrogenic differentiation of mesenchymal stem cells is inhibited after magnetic labeling with fermoxides. *Blood* **104,** 3410–3412; 3412–3413
18. Bulte, J., Duncan, D., and Frank, J. A. (2002) In vivo magnetic resonance tracking of magnetically labeled cells after transplantation. *J. Cereb. Blood Flow Metab.* **22,** 899–907
19. Dodd, S. J., Williams, M., Suhan, J. P., Williams, D. S., Koretsky, A. P., and Ho, C. (1999) Detection of single mammalian cells by high-resolution magnetic resonance imaging. *Biophys. J.* **76,** 103–109
20. Foster-Gareau, P. C., Heyn, C., Alejski, A., and Rutt, B. K. (2003) Imaging single mammalian cells with a 1.5 T clinical MRI scanner. *Magn. Res. Med.* **49,** 968–971
21. Hilderbrand, S. A., Kelly, K. A., Weissleder, R., and Tung, C. H. (2005) Monofunctional near-infrared fluorochromes for imaging applications. *Bioconjug. Chem.* **16,** 1275–1281
22. Lewin, M., Carlesso, N., Tung, C. H., Tang, X. W., Cory, D., Scadden, D. T., and Weissleder, R. (2000) Tat peptide-derivatized magnetic nanoparticles allow in vivo tracking and recovery of progenitor cells. *Nat. Biotechnol.* **18,** 410–414
23. Arbab, A. S., Wilson, L. B., Ashari, P., Jordan, E. K., Lewis, B. K., and Frank, J. A. A. (2005) Model of lysosomal metabolism of dextran coated superparamagnetic iron oxide (SPIO) nanoparticles: implications for cellular magnetic resonance imaging. *NMR Biomed.* **18,** 383–389
24. Arbab, A. S., Bashaw, L. A., Miller, B. R., Jordan, E. K., Lewis, B. K., Kalish, H., and Frank, J. A. (2003) Characterization of biophysical and metabolic properties of cells labeled with superparamagnetic iron oxide nanoparticles and transfection agent for cellular MR imaging. *Radiology* **229,** 838–846
25. Briley-Saebo, K. C., Johansson, L. O., Hustvedt, S. O., Haldorsen, A. G., Bjørnerud, A., Fayad, Z. A., and Ahlstrom, H. K. (2006) Clearance of iron oxide particles in rat liver: effect of hydrated particle size and coating material on liver metabolism. *Invest. Radiol.* **41,** 560–571
26. Terrovitis, J. V., Bulte, J. W., Sarvananthan, S., Crowe, L. A., Sarathchandra, P., Batten, P., Sachlos, E., Chester, A. H., Czernuszka, J. T., Firmin, D. N., Taylor, P. M., and Yacoub, M. H. (2006) Magnetic resonance imaging of ferumoxide-labeled mesenchymal stem cells seeded on collagen scaffolds-relevance to tissue engineering. *Tissue Eng.* **12,** 2765–2775
27. Ko, I. K., Song, H. T., Cho, E. J., Lee, E. S., Huh, Y. M., and Suh, J. S. (2007) In vivo MR imaging of tissue-engineered human mesenchymal stem cells transplanted to mouse: a preliminary study. *Ann. Biomed. Eng.* **35,** 101–108
28. Cao, F., Sadrzadeh Rafie, A. H., Abilez, O. J., Wang, H., Blundo, J. T., Pruitt, B., Zarins, C., and Wu, J. C. (2007) In vivo imaging and evaluation of different biomatrices for improvement of stem cell survival. *J. Tissue Eng. Regen. Med.* **1**, 465–468
29. Luker, G. D., and Luker, K. E. (2008) Optical imaging: current applications and future directions. *J. Nucl. Med.* **49,** 1–4
30. Blake, P., Johnson, B., and Van Meter, J. W. (2003) Positron emission tomography (PET) and single photon emission computed tomography (SPECT): clinical applications [state of the art]. *J. Neuroopthalmol.* **23,** 34–41

Received for publication March 3, 2008.
Accepted for publication July 10, 2008.